which they reside [25]. Second, solid and particulate surfaces exhibit spectral features in the thermal IR domain due to a spectral dependence of the surfaces' emissivity [e.g., 26,27].

Careful laboratory studies have shown that the coloring agent in certain Mars analog Hawaiian palagonitic soils is nanophase iron oxide [18,19,28]. We have measured the emissivity of two Mauna Kea palagonitic soils whose transmission spectra exhibit different spectral features [29] and of a thermally altered volcanic tephra sample that exhibits a wide range of crystallinity and degree of alteration (from black cinders to fully hematitic) [19]. Both of these samples may represent analogs for formation mechanisms involving the production of highly altered secondary weathering products on Mars. The emission spectra of all samples were measured at the TES spectroscopy laboratory [30] at Arizona State University with the cooperation of Dr. P. Christensen. The data were converted to emissivity using blackbody measurements combined with measurements of each sample at different temperatures [31].

**Results:** Emissivity spectra for coarse and fine particle size separates of each sample are shown in Fig. 1. Several trends are immediately obvious. First, the finer particle size fractions exhibit increasingly lower emissivity than the coarser sizes at wavenumbers above 1400 cm$^{-1}$. This effect may be a manifestation of the increased importance of multiple scattering at these frequencies rather than Fresnel-like reflections at lower frequencies. Second, emissivity peaks in the 1000–1400 cm$^{-1}$ region in the fine fraction samples are shifted to higher frequencies relative to the same feature in the coarse fraction samples. This may be a particle size effect or it may be due to variations in the silicate and/or Fe-bearing mineralogy between the coarse and fine samples [e.g., 19]. While we do not make specific mineralogic assignments for the various spectral features seen in these data, we note that a broad emissivity peak possibly due to silicates is present near 1200–1300 cm$^{-1}$ and that narrower features near 1400–1600 cm$^{-1}$ and near 400 cm$^{-1}$ are possibly consistent with crystalline iron oxide minerals like hematite and/or goethite [32].

This preliminary study has demonstrated that naturally occurring palagonites, thought to be good visible to near-IR spectral analogs for Mars, exhibit complex emissivity spectra at thermal wavelengths. Disentangling the various spectral signatures that make up the emissivity spectra of these complex assemblages may prove quite important in the interpretation of the Mars Observer TES data and of other mid-IR Mars datasets.

**References:** [1] Hargraves R. B. et al. (1977) *JGR*, 82, 4547. [2] Toulmin P. et al. (1977) *JGR*, 82, 4625. [3] Clark B. C. et al. (1977) *JGR*, 82, 4577. [4] Clark B. C. et al. (1982) *JGR*, 87, 10059. [5] Soderblom L. A. (1992) in *Mars* (H. H. Kieffer et al., eds.), 557. [6] Roush T. L. et al. (1993) in *Remote Geochemical Analysis* (C. Pieters and P. Englert, eds.), 367. [7] Soderblom L. A. et al. (1978) *Icarus*, 34, 446. [8] McCord T. E. et al. (1982) *JGR*, 87, 10129. [9] Adams J. B. et al. (1986) *JGR*, 91, 8098. [10] Arvidson R. E. et al. (1989) *JGR*, 94, 1573. [11] Murchie S. et al. (1993) *Icarus*, in press. [12] Mustard J. F. et al. (1993) *JGR*, 98, 3387. [13] Pollack J. B. et al. (1977) *JGR*, 82, 4479. [14] Morris R. V. and Lauer H. V. Jr. (1990) *JGR*, 95, 5101. [15] Morris R. V. et al. (1989) *JGR*, 94, 2760. [16] Singer R. B. et al. (1979) *JGR*, 87, 10159. [17] Evans D. L. and Adams J. B. (1980) *LPS XI*, 757. [18] Morris R. V. et al. (1990) *JGR*, 95, 14427. [19] Bell J. F. III et al. (1993) *JGR*, 98, 3373. [20] Banin A. (1992) *LPI Tech. Rept. 92-04*, 1. [21] Morris R. V. et al. (1985) *JGR*, 90, 3126. [22] Bell J. F. III et al. (1990) *JGR*, 95, 14447. [23] Hargraves R. B. et al. (1979) *JGR*, 84, 8379. [24] Bell J. F. III (1992) *Icarus*, 100, 575. [25] Toon O. B. et al. (1977) *Icarus*, 30, 663. [26] Salisbury J. W. and Eastes J. W. (1985) *Icarus*, 64, 586. [27] Salisbury J. W. et al. (1987) *JGR*, 92, 702. [28] Golden D. C. et al. (1993) *JGR*, 98, 3401. [29] Roush T. L. (1992) *LPI Tech. Rpt. 92-04*, 32. [30] Anderson D. L. et al. (1991) *LPS XXII*, 21. [31] Christensen P. R. and Harrison S. T. (1993) *JGR*, submitted. [32] Salisbury J. W. et al. (1991) *Infrared (2.1–25 μm) Spectra of Minerals*, 267, Johns Hopkins Univ.

N94-33194

42

# THERMAL STUDIES OF MARTIAN CHANNELS AND VALLEYS USING TERMOSKAN DATA: NEW RESULTS.

B. H. Betts[1,2] and B. C. Murray[1], [1]Mail Code 170-25, California Institute of Technology, Pasadena CA 91125, USA, [2]Now at San Juan Capistrano Research Institute, 31872 Camino Capistrano, San Juan Capistrano CA 92675, USA.

The Termoskan instrument onboard the Phobos '88 spacecraft acquired the highest-spatial-resolution thermal data ever obtained for Mars [1–3]. Included in the thermal images are 2 km/pixel midday observations of several major channel and valley systems (see Fig. 1), including significant portions of Shalbatana Vallis, Ravi Vallis, Al-Qahira Vallis, Ma'adim Vallis, the channel connecting Valles Marineris with Hydraotes Chaos, and channel material in Eos Chasma. Termoskan also observed small portions of the southern beginnings of Simud, Tiu, and Ares Valles and some channel material in Gangis Chasma. Simultaneous broad band visible data were obtained for all but Ma'adim Vallis. Here we present new results that go beyond the analysis presented in [4].

We find that most of the channels and valleys have higher inertias than their surroundings, consistent with Viking IRTM-based thermal studies of martian channels [e.g., 5–8]. We see for the first time that thermal inertia boundaries closely match all flat channel floor boundaries. Combining Termoskan thermal data, relative observations from Termoskan visible channel data, Viking absolute bolometric albedos from [9], and a thermal model of the Mars surface based upon [10], we have derived lower bounds on channel thermal inertias. Lower bounds on typical channel thermal inertias range from 8.4 to 12.5 (10$^{-3}$ cal cm$^{-2}$ s$^{-1/2}$ K$^{-1}$) (352 to 523 in SI units). Lower bounds on inertia differences with the surrounding heavily cratered plains range from 1.1 to 3.5 (46 to 147 in SI units).

Atmospheric and geometric effects are not sufficient to cause the inertia enhancements. We agree with previous researchers [5,6,8] that localized, dark, high inertia areas within channels are likely eolian in nature. However, the Termoskan data show that eolian deposits do not fill the channels, nor are they responsible for the overall thermal inertia enhancement, contrary to the IRTM-based conclusions of [6] and [8]. Thermal homogeneity and strong correlation of thermal boundaries with the channel floor boundaries lead us to favor noneolian overall explanations.

Higher inertia channel floors do not appear to be associated with catastrophic flood channels, although very few of these were observed. Eastern Ravi and southern Ares Vallis are the only two major channel segments observed that are not thermally distinct. They do not have flat floors. In contrast, channel floor inertia enhancements are strongly associated with channels showing fret-
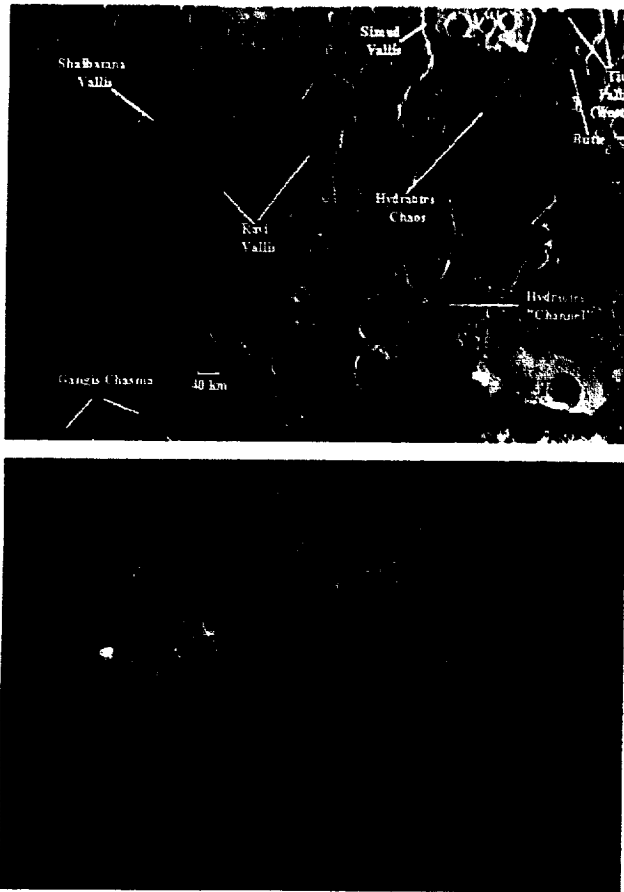
**Fig. 1.** Termoskan thermal (top) and visible (bottom) images centered approximately upon 1°S, 39°W. North is top. In the thermal image, darker is cooler. Shalbatana, Simud, and Tiu Valles all continue for several hundred kilometers north of this image. Note the cool and generally uniform floors of all channels except the eastern (and rough floored) end of Ravi Vallis. The thermal boundaries closely match the boundaries of the channel floors and depart significantly from albedo boundaries seen in the visible image. Note also the dark, presumably eolian deposits localized within the southern portions of Shalbatana Vallis and the southwestern portion of Hydraotes Chaos and spreading onto the surrounding plains in both cases. Buttes within the channels appear similar in temperature and appearance to the surrounding plains, not the channels. See, for example, the butte in the northeast corner of the image.

ting morphologies such as wide, flat floors and steep, scalloped walls. Therefore, we favor fretting processes over catastrophic flooding for explaining the inertia enhancements. Fretting may have emplaced more blocks on channel floors or caused increased bonding of fines due to increased availability of water. Alternatively, postchannel formation water that was preferentially present due to the low, flat fretted floors may have enhanced bonding of original fines or dust fallout.

Extended areal coverage from future missions will determine whether fretting is globally associated with enhanced channel floor inertias. In addition, future missions will be able to distinguish between our hypotheses for the small-scale causes of the inertia enhancements. Finally, we note that thermally distinctive channel floors represent interesting locations for future landers due to their

unique history and the probable surface presence of material from various stratigraphic layers and locations.

**References:** [1] Murray B. C. et al. (1991) *Planetary and Space Science, 39, 1/2,* 237–265. [2] Selivanov A. S. et al. (1989) *Nature, 341,* 593–595. [3] Betts B. H. (1993) Ph.D. thesis, Caltech. [4] Betts B. H. and Murray B. C. (1993) *LPS XXIV,* 103–104. [5] Christensen P. R. and Kieffer H. H. (1979) *JGR, 84,* 8233–8238. [6] Zimbelman J. R. (1986) in *Symposium on MECA,* 112–114, LPI. [7] Zimbelman J. R. and Leshin L. A. (1987) *Proc. LPSC 17th,* in *JGR, 92,* E588–E596. [8] Craddock R. A. et al. (1988) *LPSC XIX,* 215–216. [9] Pleskot L. K. and Miner E. D. (1981) *Icarus, 45,* 179–201. [10] Clifford S. M. et al. (1987) Lunar and Planetary Institute.

# THE IMPORTANCE OF ENVIRONMENTAL CONDITIONS IN REFLECTANCE SPECTROSCOPY OF LABORATORY ANALOGS FOR MARS SURFACE MATERIALS.

J. Bishop[1], S. Murchie[2], S. Pratt[1], J. Mustard[1], and C. Pieters[1], [1]Brown University, Providence RI 02912, USA, [2]LPI, Houston TX 77058, USA.

Reflectance spectra are presented here for a variety of particulate, ferric-containing analogs to martian soil ($Fe^{3+}$-doped smectites and palagonites) to facilitate interpretation of remotely acquired spectra. The analog spectra were measured under differing environmental conditions to evaluate the influence of exposure history on water content and absorption features due to $H_2O$ in these samples. Each of these materials contains structural OH bonded to metal cations, adsorbed $H_2O$, and bound $H_2O$ (either in a glass, structural site, or bound to a cation). Previous experiments involving a variety of Mars analogs have shown that the 3-μm $H_2O$ band in spectra of palagonites is more resistant to drying than the 3-μm $H_2O$ band in spectra of montmorillonites [1]. Other experiments have shown that spectra of ferrihydrite and montmorillonites doped with ferric sulfate also contain sufficient bound $H_2O$ to retain a strong 3-μm band under dry conditions [2,3]. Once the effects of the environment on bound water in clays, oxides, and salts are better understood, the hydration bands measured via reflectance spectroscopy can be used to gain information about the chemical composition and moisture content of real soil systems. Such information would be especially useful in interpreting observations of Mars where subtle spatial variations in the strengths of metal-OH and $H_2O$ absorptions have been observed in telescopic [4] and ISM [5,6] spectra.

**Experimental Procedures:** We measured bidirectional reflectance spectra of several Mars soil analogs under controlled environmental conditions to assess the effects of moisture content on the metal-OH and $H_2O$ absorptions. The samples analyzed include chemically altered montmorillonites, ferrihydrite, and palagonites from Hawaii and Iceland. Procedures for preparation of the cation-exchanged montmorillonites, ferric-salt doped montmorillonites, and ferric oxyhydroxides are described in detail elsewhere [2,3].

One set of experiments involved desiccating the samples by heating. Reflectance spectra were measured initially for these samples under humidified conditions and under $N_2$ purged of $H_2O$ and $CO_2$. The samples were then heated in an oven to 175°C at a rate of 1°C/min, cooled in a desiccator and measured again. This procedure was repeated for heating the samples to 275°C. Water contents for these samples were measured independently using thermal gravimetric analysis.